Climate Dynamics

La Plata Basin precipitation variability in spring: Role of remote SST forcing as simulated by GCM experiments

--Manuscript Draft--

Manuscript Number:	CLIDY-D-12-00435R2
Full Title:	La Plata Basin precipitation variability in spring: Role of remote SST forcing as simulated by GCM experiments
Article Type:	Original Article
Keywords:	LPB precipitation hydroclimate variability remote SST forcing AMIP-type experiments
Corresponding Author:	Annalisa Cherchi, Ph.D. CMCC/INGV Bologna, ITALY
Corresponding Author Secondary Information:	
Corresponding Author's Institution:	CMCC/INGV
Corresponding Author's Secondary Institution:	
First Author:	Annalisa Cherchi, Ph.D.
First Author Secondary Information:	
Order of Authors:	Annalisa Cherchi, Ph.D.
	Andrea F Carril, PhD
	Claudio G Menendez, PhD
	Laura Zamboni, PhD
Order of Authors Secondary Information:	
Abstract:	An ensemble of nine experiments with the same interannually varying sea surface temperature (SST), as boundary forcing, and different initial conditions is used to investigate the role of tropical oceans in modulating precipitation variability in the region of La Plata Basin (LPB). The results from the ensemble are compared with a 20th-century experiment performed with a coupled ocean-atmosphere model, sharing the same atmospheric component. A rotated empirical orthogonal functions analysis of South America precipitation shows that the dominant mode of variability in spring is realistically captured in both experiments. Its principal component (RPC1) correlated with global sea surface temperature (SST) and atmospheric fields identify the pattern related to El Niño Southern Oscillation and its large-scale teleconnections. Overall the pattern is well simulated in the tropical southern Pacific Ocean, mainly in the ensemble, but it is absent or too weak in other oceanic areas. The coupled model experiment shows a more realistic correlation in the subtropical South Atlantic where air-sea interactions contribute to the relationship between LPB precipitation and SST. The correspondence between model and data is much improved when the composite analysis of SST and atmospheric fields is done over the ensemble members having an RPC1 in agreement with the observations: the improvement relies on avoiding climate noise by averaging only over members that are statistically similar. Furthermore, the result suggests the presence of a high level of uncertainty due to internal atmospheric variability. The analysis of some individual years selected from the model and data RPC1 comparison reveals interesting differences among rainy springs in LPB. For example, 1982, which corresponds to a strong El Niño year, represents a clean case with a distinct wave train propagating from the central Pacific and merging with another one from the southeastern tropical Indian Ocean. The year 2003 is an example of a rainy spring in LPB not directly driven by remote SST forcing. In this case the internal

	variability has a dominant role, as the model is not able to reproduce the correct local precipitation pattern.

CLIDY-D-12-00435 R1 - Revision

"La Plata Basin precipitation variability in spring: Role of remote SST forcing as simulated by GCM experiments"

Annalisa Cherchi, Andrea F Carril, Claudio Menendez, Laura Zamboni

We revised the manuscript to address the reviewer comment, see the details below.

Reviewer #2

The authors addressed all my previous comments and the manuscript has improved substantially in this revised version. In my opinion, the manuscript can be accepted for publication subject of the following clarification.

In Table 3, the authors show the correlation coefficient between Nino3.4 Index and PC1 timeseries for each AMIP-style run and then calculate the "mean of correlation coefficients". I wonder how this mean was computed, as averaging correlation values has no meaning. I suggest them to see Faller, 1981, J. Appl. Meteor., for reference.

We understand the reviewer comment, and we agree that computing the mean of correlation coefficients is not mathematically correct. As we never commented that value in the text, we decided to revise the manuscript removing it from Table 3 and changing the caption of the table accordingly.

La Plata basin precipitation variability in spring: Role of remote SST forcing as simulated by GCM experiments*

Annalisa Cherchi[1], Andrea F. Carril[2,3,4], Claudio G. Menéndez[2,3,4], and Laura Zamboni[5]

[1]Centro Euromediterraneo sui Cambiamenti Climatici, and Istituto Nazionale di Geofisica e Vulcanologia, Bologna, Italy
[2]Centro de Investigaciones del Mar y de la Atmósfera (CIMA), CONICET-UBA, Buenos Aires, Argentina
[3]Departamento de Ciencias de la Atmósfera y los Océanos (DCAO), FCEN, Universidad de Buenos Aires, Argentina
[4]UMI IFAECI/CNRS, Buenos Aires, Argentina
[5]Mathematics and Computer Science Division, Argonne National Laboratory, Argonne, IL, USA

Manuscript submitted to

Climate Dynamics

April 2, 2013

Corresponding author:
Annalisa Cherchi (CMCC/INGV)
Viale Aldo Moro 44
40127 Bologna, Italy
E-mail: annalisa.cherchi@bo.ingv.it
Phone: +39 051 3782613
Fax: +39 051 3782655

Abstract

An ensemble of nine experiments with the same interannually varying sea surface temperature (SST), as boundary forcing, and different initial conditions is used to investigate the role of tropical oceans in modulating precipitation variability in the region of La Plata Basin (LPB). The results from the ensemble are compared with a 20th-century experiment performed with a coupled ocean-atmosphere model, sharing the same atmospheric component. A rotated empirical orthogonal functions analysis of South America precipitation shows that the dominant mode of variability in spring is realistically captured in both experiments. Its principal component (RPC1) correlated with global sea surface temperature (SST) and atmospheric fields identifies the pattern related to El Niño Southern Oscillation and its large-scale teleconnections. Overall the pattern is well simulated in the tropical southern Pacific Ocean, mainly in the ensemble, but it is absent or too weak in other oceanic areas. The coupled model experiment shows a more realistic correlation in the subtropical South Atlantic where air-sea interactions contribute to the relationship between LPB precipitation and SST. The correspondence between model and data is much improved when the composite analysis of SST and atmospheric fields is done over the ensemble members having an RPC1 in agreement with the observations: the improvement relies on avoiding climate noise by averaging only over members that are statistically similar. Furthermore, the result suggests the presence of a high level of uncertainty due to internal atmospheric variability. The analysis of some individual years selected from the model and data RPC1 comparison reveals interesting differences among rainy springs in LPB. For example, 1982, which corresponds to a strong El Niño year, represents a clean case with a distinct wave train propagating from the central Pacific and merging with another one from the eastern tropical south Indian Ocean. The year 2003 is an example of a rainy spring in LPB not directly driven by remote SST forcing. In this case the internal variability has a dominant role, as the model is not able to reproduce the correct local precipitation pattern.

1 Introduction

La Plata basin (LPB) is a region in southeastern South America (SESA), comprising southern Brazil, Uruguay, northeastern Argentina, southern Paraguay, and southern Bolivia, that strongly relies on agriculture and hydro-electric power. The region is a key area for the variability of the precipitation over South America having high values in all the seasons (see Zamboni et al., 2010).

At interannual timescales LPB precipitation has been linked to El Niño Southern Oscillation (ENSO) with a clear seasonality in the connection (Aceituno, 1988; Grimm et al., 2000; Paegle and Mo, 2002; Grimm, 2003; Cazes-Boezio et al., 2003; Vera et al., 2006; Barreiro, 2010, among others). El Niño influences SESA involving both upper and lower-level circulation anomalies: increased seasonal precipitation develops over LPB, while the northeast South America experiences drier conditions, and during La Niña the sign of the anomalies is reversed (Grimm et al., 2000). In the upper levels, Rossby wave trains propagating from the equatorial Pacific influence baroclinicity and advection of cyclonic vorticity over SESA (Yulaeva and Wallace, 1994; Grimm et al., 2000). In the lower levels, anomalous intensity and direction of the South American low-level jet may change the moisture variability (i.e. Liebmann et al., 2004; Silvestri, 2004). The season with the best established teleconnection between ENSO and LPB hydro-climate is austral spring (Pisciottano et al., 1994; Grimm et al., 1998; Cazes-Boezio et al., 2003; Barreiro, 2010; Zamboni et al., 2012).

The efforts to explain SESA precipitation variability have been based on both observations and model analysis. Comparison of the performance of IPCC AR4 coupled general circulation models (CGCMs) in simulating SESA precipitation and its variability reveal that they have problems in representing accurately the variability associated with the South Atlantic Convergence Zone (SACZ), but models having a good ENSO tend also to have a good teleconnection in South America (e.g. Silvestri and Vera, 2008; Vera and Silvestri, 2009). Atmospheric general circulation models (AGCMs) forced with prescribed sea surface temperature (SST) have been tested as well, analyzing precipitation and circulation biases over South America (Zhou and Lau, 2002), investigating the remote forcing from different ocean basins for predictability issues (Taschetto and Wainer, 2008; Barreiro, 2010), or assessing their ability to reproduce the past history of SESA

precipitation (Seager et al., 2010).

The SST of tropical oceans could affect the climate of South America through different mechanisms, such as (i) Rossby wave trains that propagate into the extratropics and then into South America, affecting its eastern regions (i.e. Paegle and Mo, 2002; Vera et al., 2004); (ii) shift and alteration of the Walker circulation (Cazes-Boezio et al., 2003); and (iii) influence of subtropical jets and southward inflow of humidity (Byerle and Paegle, 2002). In the present study we investigate the influence from remote forcing (i.e., mainly SST) following the mechanisms just described. In particular, performances of atmosphere-only and atmosphere-ocean coupled models are investigated and compared in terms of hydro-climate variability over SESA at interannual timescale. The analysis focuses mostly on austral spring when the connection between ENSO and LPB precipitation is known and well established. A large ensemble of AMIP-type experiments with the same boundary forcing (i.e., interannually varying SST) and different initial conditions is analyzed in terms of the correspondence between model and data leading principal components (PC1s). By means of that comparison specific case studies have been selected and analyzed in more detail in terms of remote SST forcing vs internal variability influences.

The study is organized as follows. Section 2 describes the model used and the experiments performed, including a list of the datasets and reanalysis used to verify the model performance. Section 3 analyzes the hydro-climate (mainly in terms of precipitation) variability and its relationship with remote SST. Section 4 investigates in more detail the characteristics of the remote SST forcing over LPB precipitation, classifying years according to empirical orthogonal functions (EOFs) model performances. Section 5 lists and analyzes selected years for remote SST forcing versus internal variability issues. Section 6 summarizes the main conclusions of the study.

2 Description of model experiments and datasets

Two kinds of experiments have been used for the present study: an ensemble of AMIP-type experiments and a 20th-century coupled model simulation. The ensemble of AMIP-type experiments consists of 9 members with the same boundary conditions, which are interannually varying SST taken from the HadISST dataset (Rayner et al., 2003), and different initial conditions. The period

analyzed is 1948-2003. The experiments have been performed with the ECHAM4 atmospheric general circulation model (Roeckner et al., 1996) at T106 horizontal resolution (corresponding to a grid of $1^\circ \times 1^\circ$) and 19 sigma vertical levels.

The 20th-century coupled model simulation (hereafter SSXX) has been performed with the coupled atmosphere-ocean general circulation model SINTEXG (Gualdi et al., 2008). It includes prescribed concentration of greenhouse gases (i.e., CO_2, CH_4, N_2O and chlorofluorocarbon) and sulfate aerosols, as specified for the 20C3M experiment defined for the IPCC AR4 simulations (see http://www-pcmdi.llnl.gov/ipcc/about_ipcc.php for more details). The characteristics of both atmospheric and oceanic model components are described in previous publications (Cherchi et al., 2008; Gualdi et al., 2008). In particular, the atmospheric component is the same used for the AMIP-type simulations. The oceanic component is OPA (Madec et al., 1998), which is spatially distributed over a three-dimensional Arakawa-C-type grid (about $2^\circ \times 2^\circ$ horizontal resolution, with a meridional refinement of 0.5° at the equator) and 31 prescribed vertical levels.

The model outputs have been compared with observations and reanalysis data. The global distribution of sea surface temperature has been taken from the HadISST dataset (Rayner et al., 2003), atmospheric fields come from the NCEP reanalysis (Kalnay et al, 1996), and the global precipitation over land is taken from the CRU dataset (Mitchell and Jones, 2005). Satellite globally distributed precipitation for the period 1979-2003 from the CMAP dataset (Xie and Arkin, 1997) has been used for comparison with and validation of the land-precipitation dataset.

3 Simulated hydro-climate variability over South America

The analysis in this section focuses on the hydro-climate variability (mostly based on precipitation) over South America, with emphasis on its southeastern part, during the austral spring (October, November, December mean; hereafter OND mean). Spring is chosen because it has the largest teleconnection with ENSO (Pisciottano et al., 1994; Grimm et al., 1998; Grimm et al., 2000; Barreiro, 2010, among others) and the largest correlation between observed and modeled LPB precipitation (not shown). Table 1 shows OND mean precipitation and its standard deviation averaged over South America (between 45°S and the Equator) and over LPB (65°-47°W, 37°-19°S)

for the CRU dataset and for the model outputs (over land points). In the AMIP-type ensemble, the computation is applied to all members as if they were a single timeserie. In the LPB region the model simulates an amount of precipitation larger than observed, but its standard deviation is smaller (Table 1). That is, the model tends to underestimate the variability of the precipitation over LPB, even if it tends to overestimate its total amount.

In the literature, precipitation variability over SESA, and over the LPB region in particular, has been measured by rainfall indices defined as averages over specific regions (Boulanger et al., 2005; Vera and Silvestri, 2009; Barreiro, 2010, among others). The area used to compute the LPB values in Table 1 corresponds to the LPB index defined in Barreiro (2010). In the AMIP-type ensemble mean that index, averaged in austral spring (OND), is significantly correlated with the analogue computed from CRU data (the correlation coefficient is 0.56), suggesting that in this season the role of the forcing from oceanic SST is large and worthy of investigation, even though a large component of internal variability remains (Zamboni et al., 2012).

Because of the model weakness in simulating the correct precipitation standard deviation, we decided to employ an index based on the EOFs of precipitation anomalies over South America. EOFs and PCs allow identifying the dominant modes of variability, avoiding the inconsistencies between model and observations in the geographical differences. In past literature the dominant modes of variability of the precipitation over South America have been investigated using different datasets. Because of the sparse distribution of the observations in many regions of South America, gridded datasets such as the CRU dataset cannot represent correctly its precipitation (Stuck et al., 2006; Carril et al., 2012), and the global precipitation coverage taken from satellite measurements after 1979 (CMAP) is possibly more reliable. Past studies reveal that over the LPB region mean fields and variances of CRU and CMAP are similar (e.g. Boulanger et al., 2005) and we intend to strengthen this result by comparing EOF patterns obtained from the two datasets.

To alleviate the orthogonality constraint and have better results in terms of physical meaning we applied rotated EOFs (REOFs) to land precipitation over South America (between 45°S and the equator) in spring for the CRU and CMAP datasets during their overlapping period of existing data (1979-2005). The number of EOFs to be rotated has been chosen by means of the rule of

thumb described in North et al. (1982). Fig. 1 shows the first three rotated EOFs. The highest variance is explained by the first mode that in both datasets corresponds to the north-south dipole in the eastern side of the continent (fig. 1a,d). The corresponding principal component (RPC1) is highly correlated between CRU and CMAP (Table 2). The higher modes also have similar patterns (fig. 1b,c and fig. 1e,f) and their PCs are significantly correlated (see the values in the diagonal of Table 2). These results give us confidence in continuing the investigation using the 50 years available in the CRU dataset to validate and compare the model results in the period 1948-2003 for the first mode.

Fig. 2(a,b) shows the first mode of variability of South America precipitation during OND, and its principal component for the CRU dataset (fig. 2c) considering the long time record (1948-2003). The dominant mode of variability is as well a north-south dipole with centers at 15°S and 30°S (fig. 2a) in the eastern part of the continent. Its first principal component (RPC1, fig. 2c) corresponds to the variability of ENSO, as the correlation coefficient between PC1 and NINO3.4 (monthly mean SST anomalies averaged in the box 5°S-5°N, 170°W-120°W) is 0.59. In the CRU dataset when changing the time record length, the first mode is unchanged, whereas the second and third seem to be inverted (not shown). The difference could be related to the modulation of the decadal variability of LPB precipitation associated with the Southern Hemisphere climate, as discussed by Silvestri and Vera (2009).

The performance of the model in reproducing the dominant modes of variability of the precipitation over South America is shown as well. The first mode in the AMIP-type experiments is a north-south dipole with centers over the LPB region and over the northeastern part of the continent (fig. 2b), which is comparable with the observations (the spatial correlation between the two REOF1 patterns is 0.60). In the AMIP-type ensemble the EOFs are computed over all the members concatenated to form a long record. Table 3 summarizes the relationship between the rotated principal component in the AMIP-type ensemble and ENSO: RPC1 is significantly correlated with the NINO3.4 index. Even in the coupled model the spatial patterns of the first mode of variability is realistic (not shown).

On the basis of these results we adopted OND RPC1 as index of precipitation variability over

LPB. Positive (negative) values correspond to wet (dry) conditions over LPB and the reverse to the north, following the intensity of the SACZ (Paegle and Mo, 2002; Liebmann et al., 2004; Silva et al., 2009). The correspondence between precipitation variability in LPB and remote SST during spring is shown in figure 3. The correlation coefficients between RPC1 and global SST identify the patterns related to ENSO and its teleconnections (fig. 3a). In fact, wet (dry) LPB years are related to positive (negative) SST anomalies in the tropical Pacific and Indian Oceans, eastern equatorial Atlantic, subtropical South Atlantic near the South American coast, and southeastern Pacific, peaking at 50°S, and with negative (positive) SST anomalies in the central North Pacific, subtropical southwestern Pacific, and southwestern South Atlantic (see also Paegle and Mo, 2002; Seager et al., 2010).

The ENSO-LPB precipitation teleconnection is strong and robust in the AMIP-type ensemble, although it presents some biases. In particular, the pattern in the Pacific Ocean (from the tropical sector to its southern part) is well represented in the ensemble in agreement with the idea of its strong forced influence (fig. 3b). Concerning the other oceanic sectors, the teleconnection is drastically weaker or absent in the North Pacific, in the subtropical South Atlantic, and in the Indian sector (fig. 3b). It is now well recognized that some patterns of SST variability result from a combination of atmospheric and oceanic processes (Deser et al., 2010) and here we compare the forced experiments results with the coupled model experiment (fig. 3c).

In the tropical Pacific Ocean (fig. 3c) the correlation tends to extend for the whole basin (up to the western edge), consistent with the well-known biases of the coupled model in the ENSO representation (Navarra et al., 2008). Similarly, in the North Pacific the coupled model misses the right connection with ENSO as it is wrongly triggered by model biases and air-sea coupling influences (Cherchi et al., 2012). In the coupled model experiment the performance improves mostly in the subtropical South Atlantic and in the Indian sector. In the latter case weak but positive values are found in the western side of the basin, in agreement with the finding that air-sea interactions are a benefit for the simulation of the variability in the area (Wu and Kirtman, 2004).

In the subtropical South Atlantic, the positive correlation is indicative of a relationship between

SACZ, LPB precipitation and SST. Looking for reproducibility and predictability patterns of South America precipitation, Taschetto and Wainer (2008) found that in the area of the SACZ closer to the continent the influence of the SST forcing on the convective activity is weak. In our experiments we find a net improvement in the simulation of the SST-LPB precipitation relationship when air-sea interactions are taken into account (i.e. in the coupled model experiment results). Therefore we argue that they are important for the variability of the region. A similar conclusion has been obtained by Barreiro (2010) for the fall season. These arguments suggest that the teleconnection between LPB precipitation and ENSO is locally modulated by the air-sea interactions in the subtropical South Atlantic. One possible route would involve cloudiness over the SACZ which affects the surface energy balance and thus influences the SST. The latter would in turn affect surface fluxes and then feedback on precipitation changes.

4 Remote SST forcing on LPB precipitation variability

Following the results from Section 3, we classified wet (dry) LPB years using the first rotated principal component (RPC1) of precipitation anomalies over South America (as defined in the previous section), choosing 1 (-1) standard deviation as the threshold. Wet (dry) LPB years are characterized by a precipitation dipole with excess (deficit) of precipitation over LPB and the reverse north of it, respectively. In this section most of the analysis is based on composite anomalies: a non-parametric statistical significance test using re-sampling technique (Wilks, 1995) is applied to them.

Figure 4 shows the composite of SST and 200 mb eddy streamfunction for wet and dry LPB years computed for the HadISST/NCEP datasets and for the AMIP-type ensemble. The shaded SST values and the thicker 200 mb streamfunction contours are statistically significant at 95%. In the observations, the SST anomalies are almost symmetric between the two phases in the tropical and south extratropical Pacific, but not in the extratropical North Pacific, in the Indian Ocean, and in the subtropical South Atlantic sectors (fig. 4a,b). In particular, wet LPB years are associated with positive SST anomalies remarkably large over the eastern tropical Pacific (Zhou and Lau, 2001; Paegle and Mo, 2002; Seager et al., 2010), but also significant over the tropical In-

dian Ocean (e.g., Taschetto and Ambrizzi, 2012) and the eastern tropical Atlantic Ocean (i.e., the Gulf of Guinea). During dry LPB years SST anomalies of opposite sign are found over the tropical southern Pacific and in the Indian Ocean, although the latter are less pronounced. Positive anomalies are observed over the extratropical North Pacific while negative anomalies exist in the subtropical South Atlantic, off the South American coast (fig. 4a,b).

In the AMIP-type ensemble the composite can be built in two ways: (1) considering the RPC1 of all members as if they were a long timeserie (i.e. as computed for fig. 2), or (2) considering the RPC1 of the ensemble mean. In the latter case the internal variability would be filtered out. SST and 200 mb streamfunction patterns are comparable in the two cases; therefore for conciseness we show only the results from the computation type as described in (1), as we did for fig. 4. SST anomalies are realistic in the tropical and southern Pacific Ocean but not in the North Pacific, tropical Indian, and Atlantic sectors (fig. 4c,d). In particular, the asymmetry between strong and weak LPB years in the North Pacific is not simulated, and the anomalies in the Indian sector are largely weaker than observed.

In the observations, in both wet and dry LPB years, a wave train propagates from the western Pacific/Indian sector, as depicted by the 200 mb eddy streamfunction (fig. 4a,b contours), and it recalls the Pacific South American (PSA) modes (Kidson, 1988; Mo and Paegle, 2001; Chan et al., 2008; Cai et al., 2011; Taschetto and Ambrizzi, 2012). These patterns are remarkably symmetric in the Southern Hemisphere (fig. 4a,b). During wet LPB years the intensities are larger in the starting propagating phase, but in the dry LPB years the positive streamfunction anomalies over SESA and adjacent Atlantic sector are more intense. Vera et al. (2004) proposed that these may originate from the central Pacific, but the amplification may also arise from local processes over SESA. Anomalies recalling the PSA can be identified in the model as well (fig. 4c,d), with the contribution from the central Pacific being more evident.

The relationship between SST in the subtropical South Atlantic and LPB precipitation is not symmetric (fig. 4a,b). In fact, in the composite SST negative anomalies and positive upper troposphere streamfunctions are found during dry LPB years, but the reverse does not occur for wet LPB years. As previously discussed, in the AMIP-type ensemble air-sea interactions are by defi-

nition not present but a realistic response is observed in the circulation for the component coming from the remote teleconnection. On the other hand in the coupled model the remote teleconnection is weaker but the SST response is realistic (not shown), even if it is exactly symmetric between dry and wet LPB years, differently from the observations.

In the AMIP-type ensemble, the model RPC1 computed by considering all members as a long timeserie permits allows each member to be compared with the observations. For each member, the model RPC1 may peak in the same years as in the observations but also in others, and considering the nine members available we can build larger samples of cases. In fact, we found that composing years according to the correspondence between AMIP-type RPC1 and observed RPC1 provides additional information on the origin of the remote SST forcing for the LPB hydroclimate. According to that for each member we have classified years as "In Phase" when the model and observation-based RPC1 exceed 1 standard deviation (std); as "Out of Phase" when the two RPC1 are of opposite sign; and as "Partial in Phase" when the two have the same sign but the model RPC1 does not exceed 1 std.

During "In Phase" years the dipole between LPB and SACZ in the precipitation is the strongest (fig. 5a,b), whereas it is barely visible during "Partial in Phase" years (fig. 5e,f). In the latter case however the anomalies over LPB, even if weaker, are of the same sign as in the "In Phase" group (fig. 5e,f). On the other hand, during the "Out of Phase" years, the precipitation composites have excess (deficit) of precipitation in the region north of the LPB without any clear signal in the southern part of the dipole (fig. 5c,d).

It is instructive to discuss the composite of SST and 200 mb eddy streamfunction built using the classification just introduced (fig. 6). As in fig. 4, shaded SST values and thicker 200 mb streamfunction contours are statistically significant at 95%. The "In Phase" composite of SST (fig. 6a,b) reflects the observed anomalies (fig. 4a,b). In fact, during wet LPB years positive SST anomalies in the central eastern Pacific are associated with positive anomalies in the Indian sector and negative anomalies in the subtropical south Pacific. On the other hand, during dry LPB years negative anomalies in the central eastern Pacific are associated with positive anomalies in the North Pacific and negative anomalies in the South Atlantic (around 30°S), off the South American

coast. The main difference exists in the subtropical Indian sector where the "In Phase" negative composite (fig. 6b) has anomalies near zero and not negative as in the observations (fig. 4b).

Similarly to the SST, the wave propagation in the "In Phase" composite corresponds to the observations (fig. 6a,b) for both wet and dry LPB years, with a clear wave train propagating from west to east. In the positive case, positive SST anomalies in the central eastern tropical Pacific are associated with positive anomalies in the Indian sector and with negative anomalies in the subtropical south Pacific in correspondence of the dateline (fig. 6a). Both conditions are present only when the positive "In Phase" cases are considered, and both seem responsible for the occurrence of the wave train. In the negative case (fig. 6b), the HadISST composite has an SST pattern just opposite, but with the negative anomalies in the Indian Ocean weaker (considering their absolute values) than in the positive case. Further, in the "In Phase" negative composite the values in the Indian Ocean are near zero (fig. 6b). Actually in this last case the wave train seems to propagate from Indonesia rather than from the eastern Indian sector as it does in the positive case. Further comparing fig. 4 and fig. 6 shows that the "Out of Phase" composite has no propagating signals (fig. 6c,d), whereas the "Partial in Phase" group has a weaker wave train that seems to propagate from the Indian (central Pacific) sector in the positive (negative) case (fig. 6e,f).

The comparison between fig. 4 and fig. 6 suggests that the forcing from SSTA in the tropical Pacific Ocean may provide both wet and dry conditions in the LPB region and that the forcing from other basins, such as the Atlantic and the Indian Oceans, may trigger the teleconnection with the Pacific. In fact, in the "Out of Phase" composite (fig. 6c,d) the SST anomalies in the tropical Pacific and Indian Ocean sectors correspond to the "In Phase" composite, whereas the anomalies in the North and subtropical South Pacific and in the Atlantic region largely differ. On the other hand, the main differences between "In Phase" and "Partial in Phase" composites in terms of SST are localized in the Indian Ocean (fig. 6e,f). The comparison between "In Phase" and "Out of Phase" composites suggests that an SST pattern with negative (positive) anomalies southwest of large positive (negative) anomalies in the tropical Pacific Ocean may have a dominant role in terms of the wave propagation of the atmospheric teleconnection from the Indian-Pacific sector to South America (Vera et al., 2004).

Shift and alteration of the Walker circulation associated with SSTA in the tropical oceans directly affect tropical South America (Cazes-Boezio et al., 2003). During warm ENSO events the Walker circulation shifts eastward and its subsiding branch occurs over South America. When the precipitation dipole is in its positive phase (i.e., rainy LPB and dry Amazon) subsidence over the Amazon is particularly evident for the "In Phase" composite, as shown from its mean vertical velocity (see Table 4). Conversely, when the dipole is in its negative phase the vertical velocity anomaly has the opposite sign, favoring convection over northern South America (Table 4). In terms of local processes over South America, the "In Phase" composite of vertically integrated (from the surface to about 200 mb) moisture shows a well-defined dipole between LPB and SACZ (fig. 7a,b). The anomalies between positive and negative phases are symmetric, and the moisture fluxes are directed northeasterly (southwesterly) in correspondence with positive (negative) moisture anomalies (fig. 7a,b). The "Out of Phase" composite shows fluxes directed in the opposite direction, and the moisture anomalies over LPB are absent or extremely weak (fig. 7c,d). In the latter case, anomalies of sign opposite to the "In Phase" composite are large in the northern part of South America (fig. 7c,d).

Over the Andes near the position of the subtropical jet (last column of Table 4), stronger upper tropospheric, subtropical westerlies (e.g., during warm ENSO events) correlate with an eastward and southward flow of humidity emanating from the Amazon basin toward LPB (Byerle and Paegle, 2002). Indeed, the positive phase of the dipole (rainy LPB) coincides with an intensification of the westerlies (Table 4), consistently with the presence of a larger moisture supply from the northwest through the low-level jet. The weakening of the subtropical jet in the negative phase suggests the occurrence of opposite dynamics (Table 4).

5 SST forcing vs internal variability: some case studies

Table 5 lists wet and dry LPB years according to the "In Phase" and "Out of Phase" groups, for each year the number of members of the ensemble sharing the same result is given in parentheses. This represents a measure of the inter-member spread. For positive RPC1 cases (i.e., wet LPB years), 1982 and 2003 are two interesting cases worthy of further investigation. In particular, 1982

is the only case having all nine members reproducing the observed result: 100% of the members have a positive RPC1 exceeding 1 standard deviation as in the observations. This case could be interpreted as the clean example of remote SST influence; moreover it corresponds to one of the strongest El Niño years in the analyzed record. Year 2003 is characterized by having eight out of nine members with a negative large RPC1 (exceeding -1 standard deviation) rather than a large positive one as found in the CRU dataset.

As mentioned in Section 3, in the observations the correlation between RPC1 and NINO3.4 is significant. When we consider OND SA precipitation RPC1 years exceeding 1 (-1) std, three out of seven (two out of eight) wet (dry) LPB years correspond with El Niño (La Niña) events. This means that only three (two) out of seven (eight) extreme wet (dry) LPB years occurred in correspondence with an El Niño (La Niña) year.

For negative RPC1 cases (i.e., dry LPB years) it is hard to identify a net common behavior among the members. We decided to focus on 1999 because it has 4 members "In Phase" and 5 members "Partial in Phase" with CRU results, and it corresponds to a La Niña year.

5.1 1982 case study

Year 1982 is the only case in our record having all members with a RPC1 larger than 1 std as in the observations. Since all members agree, we expect that the LPB precipitation pattern is completely forced from remote SST distribution. Fig. 8b shows the precipitation pattern in the AMIP-type ensemble merging all 1982 years, which consists of a well-defined dipole with excess of precipitation over LPB and deficit north of it, associated with a low-level convergence. In terms of SST, 1982 represents one of the strongest El Niño years in recent record and consists of large positive SSTA (above 2.4°C) in the eastern tropical Pacific Ocean (fig. 8a). During that year, positive SSTA in the tropical Pacific region are associated with negative SSTA in the subtropical Pacific around the dateline (both north and south of the equator), weak positive anomalies in the western Indian Ocean and negative anomalies in the equatorial and subtropical South Atlantic. In the model, this SST pattern produces a clean wave train propagating from the central Pacific and merging with the other one propagating from eastern tropical South Indian Ocean (fig. 8a). Over South America, the

200 mb streamfunction north of 20°S is positive, in agreement with the observations (not shown), whereas it is negative (positive) south of it in the east (west), different from the observations (not shown). In this case, the simulated precipitation anomalies over LPB can be interpreted as a net consequence of the teleconnection from the Pacific-Indian Ocean sectors.

5.2 2003 case study

A case opposite to that of 1982 is 2003 because the AMIP-type ensemble members mostly agree in simulating a precipitation pattern opposite to the one observed. In fact, eight members out of nine have a large and negative RPC1 (Table 5) associated with slight negative precipitation over LPB and large positive values in the northeast (fig. 9d), instead of large positive rainfall over LPB and the opposite in the north as observed (fig. 9b).

Year 2003 is not an El Niño year and it experienced SST anomalies generally warmer than the mean climatology in all tropical basins (fig. 9a,c). The temperature values were not large but they were almost zonally uniform in the tropics. Considering this SST distribution, a teleconnection from the Pacific cannot be responsible for the rainfall pattern over South America. In fact the 200 mb eddy streamfunction show a pattern with cyclones and anticyclones east of 120°W (fig. 9a, contours) recalling the quasi-stationary anomalous circulation over the south eastern south Pacific Ocean described by Solman and Orlanski (2009). According to that, the dipole precipitation pattern over South America could be explained by the anomalous high and associated circulation and by moisture convergence (Liebmann et al., 2004; Solman and Orlanski, 2009).

In the AMIP-type ensemble, the wave pattern is not captured (fig. 9c, contours) and intense continental precipitation is displaced north of 30°S (fig. 9d). In the model, the internal variability and the associated spread among the ensemble members seem to dominate the response over South America with a signal to noise ratio that varies year to year. In fact, only one of nine members is able to reproduce the observed wave pattern in the southeastern South Pacific sector (fig. 10), with a streamfunction at 200 mb highly variable among the members (fig. 10l).

5.3 1999 case study

Year 1999 experienced a strong La Niña with large negative SSTA in the tropical central and eastern Pacific Ocean (fig. 11a,c). Over South America dry (wet) conditions occur over LPB (north of it) (fig. 11b). In the model ensemble, four and five members have a RPC1 "In Phase" and "Partial in Phase", respectively, with the CRU RPC1. The model average of these members reproduces the observed dipole, but the values are weaker than observed (fig. 11d).

In the upper troposphere, eddy streamfunction anomalies form a quadruple in the western Pacific and continental sectors (fig. 11a,c). In both model and observations a wave train propagates from the tropical western Pacific, and positive anomalies are localized over LPB and adjacent ocean (fig. 11a,c). The latter in the model is weaker than observed.

To verify the inter-member performance, we plot in fig. 12 precipitation and 200 mb eddy streamfunction anomalies during OND for each member. The members presenting a clear dipole and negative precipitation anomalies over LPB have positive 200 mb eddy streamfunction anomalies over subtropical South America, as well as a quadruple between western Pacific and American continental sectors (fig. 12b,f,h,i). However these patterns over subtropical South America appear to originate from the internal variability: the inter-members standard deviation of 200 mb streamfunction has a maximum over LPB (fig. 12l), consistent with the finding of Zamboni et al. (2012).

6 Conclusions

We studied the influence of tropical SST anomalies on the precipitation variability over LPB in spring, analyzing an ensemble of AMIP-type experiments. Each experiment is built with the ECHAM4 atmospheric GCM at relatively high horizontal resolution (i.e., $1^\circ \times 1^\circ$) forced with interannually varying SST from 1948 to 2003. The ensemble consists of nine members differing in terms of initial conditions. To explore the potential importance of ocean-atmosphere interaction, we compare the AMIP-type ensemble with a 20th-century experiment performed with a coupled model sharing the same atmospheric component. The study is focused on austral spring, a choice motivated by the fact that during this season the signal from the tropical Pacific is more robust (e.g., Pisciottano et al., 1994; Grimm et al., 1998; Grimm et al., 2000; Barreiro, 2010).

Both atmospheric and coupled models perform well in terms of seasonal mean precipitation and its standard deviation over LPB and South America, although the seasonal mean is slightly overestimated and its variability somewhat underestimated. The analogue computed from observations is significantly correlated with the values obtained from the SST-forced ensemble, evidencing that oceans influence the precipitation over LPB.

Although a relatively high level of uncertainty in the observations characterizes large areas of South America (Carril et al., 2012), our results indicate that the regional climate modes of variability calculated from two independent precipitation databases (CRU and CMAP) for 1979-2003 are similar. Therefore we use the longer period (1948-2003) of CRU precipitation to validate the broad-scale regional modes of variability during austral spring in the model.

The spatial pattern of the dominant mode of variability of precipitation over South America is realistically captured by the models. The first mode, obtained by a rotated EOF analysis, is a south-north precipitation anomaly dipole with centers over LPB and central-northern Brazil, and its principal component (RPC1) is used as index of the precipitation interannual variability. Its correlation with global SST identifies the patterns related to ENSO and its known teleconnections. The teleconnection pattern in the southern Pacific Ocean is well captured in the SST-forced ensemble, but it is absent or too weak in other oceanic areas. The correlation in the subtropical South Atlantic is more realistic in the coupled model experiment: in this case air-sea feedbacks contribute to better capture the relationship between precipitation and SST. Specific sensitivity experiments would aid in better characterizing this aspect.

Composite fields of upper-tropospheric streamfunction anomalies averaged over all wet springs in SESA consist in wave trains extending southeastward from the eastern Indian Ocean and Indonesia before they turn equatorward into South America. The dry composite is almost symmetric in the tropical and southern Pacific. These wave trains share some elements of the second and third leading modes of Southern Hemisphere circulation variability on interannual time. The SST-forced ensemble captures the circulation anomalies and also those of SST in the tropical and southern Pacific, but the anomalies are of lower amplitude than observed.

When the composite for wet/dry events is done by averaging only over those ensemble members

for which the model and observations agree on the occurrence of strong positive/negative precipitation anomalies ("In Phase" composite), then the structure of teleconnections better corresponds with the observed one. This improvement arises from avoiding the climate noise by averaging only over members that are statistically similar. The SST anomalies in the Indian Ocean (correctly captured in the "In Phase" composite) seems to be a factor to take into account since it is in this sector where the wave train influencing the precipitation dipole in South America appears to originate.

We analyzed some individual springs comparing the RPC1 of the model and of the observed data in terms of the number of ensemble members in agreement with observations. In the spring of 1982 rainfall anomaly is a dipole between LPB and SACZ, and all members agree with the observations. The associated SST pattern produces a clean wave train propagating from the central Pacific and merging with another one propagating from the eastern tropical South Indian Ocean. In 1982 a strong El Niño event occurred. For other El Niño or La Niña events however the agreement between the ensemble members in the simulation of the rainfall dipole was not as striking as in 1982. Reasons behind this discrepancy could be ascribed to unclear teleconnections (i.e., large dispersion between simulated members) or to the SST intensities (i.e., 1982 anomalies were much larger in absolute value than 1999 ones). We also note that only some too rainy or too dry LPB springs are associated with the occurrence of El Niño or La Niña.

A rainy spring for SESA was 2003, but in this case almost all ensemble members exhibit a precipitation dipole out of phase with respect to the observations (from this point of view this case is opposite that of 1982). This year exhibits a zonally symmetric pattern of moderately positive SST anomalies throughout the tropics. In this case, the ensemble mean does not exhibit any teleconnection through the South Pacific. Not having sectors with well-defined anomalously warm pools in the tropics is a source of additional uncertainty in the simulation of the southern hemisphere extratropics since wave trains propagating through the Southern Oceans are not excited uniformly in the different ensemble members (large inter-member spread in the circulation).

Tropical ocean SST and associated remote teleconnections are crucial for the hydro-climate variability over LPB. The results presented attest how remote SST forcing and internal variability

may influence the precipitation variability over the region when considering some selected years in terms of the performance of the model used. Our finding support the idea that seasonal climate forecasts based on numerical techniques rather than on purely empirical relationships (i.e. with SST) are necessary.

Acknowledgements. We are grateful to the two anonymous reviewers for their useful comments. The research leading to these results has received funding from the European Community's Seventh Framework Programme (FP7/2007-2013) under Grant Agreement N° 212492 (CLARIS LPB. A Europe-South America Network for Climate Change Assessment and Impact Studies in La Plata Basin). Dr AF Carril and Dr CG Menéndez were partially supported by PIP 112-200801-01788 (CONICET, Argentina) and PICT 2008-00237 (FONCYT, Argentina). The Italian Ministry of Education, University and Research, and Ministry for Environment, Land and Sea through the project GEMINA is gratefully acknowledged for the support to Dr A Cherchi. Dr L Zamboni was partially supported by American Recovery and Reinvestment Act (ARRA) funding through the Office of Advanced Scientific Computing Research, Office of Science, U.S. Dept. of Energy, under Contract # DE-AC02-06CH11357.

References

Aceituno P (1988) On the functioning of the Southern Oscillation in the South American sector. Part I: Surface climate. Mon Wea Rev, 116, 505-524

Barreiro M (2010) Influence of ENSO and the South Atlantic Ocean on climate predictability over south-eastern South America. Clim Dyn, 35, 1493–1508 DOI:10.1007/s00382-009-0666-9

Boulanger JP, J Leloup, O Penalba, M Rusticucci, F Lafon, W Vargas (2005) Observed precipitation in the Parana-Plata hydrological basin: long-term trends, extreme conditions and ENSO teleconnections. Clim Dyn 24: 393–413

Byerle LA, Paegle J (2002) Description of the seasonal cycle of low-level flows flanking the Andes and their interannual variability. Meteorol 27: 71–88

Cai W, van Rensch P, Cowan T, Hendon HH (2011) Teleconnection pathways of ENSO and the IOD and the mechanisms for impacts on Australian rainfall. J Clim 24: 3910–3923

Carril AF, and co-authors (2012) Performance of a multi-RCM ensemble for South Eastern South America. Clim Dyn 39: 2747–2768

Cazes-Boezio G, Robertson AW, Mechoso CR (2003) Seasonal dependence of ENSO teleconnections over South America and relationships with precipitation in Uruguay. J Climate, 16, 1159-1176

Chan SC, Behera SK, Yamagata T (2008) Indian Ocean dipole influence on south American rainfall. Geophys Res Lett 35 L14S12 doi:10.1029/2008GL034204

Cherchi A, Masina S and Navarra A (2011) Tropical Pacific-North Pacific teleconnection in a coupled GCM: Remote and local processes. Int J Climatol 32: 1640–1653

Cherchi A, Masina S and Navarra A (2008) Impact of extreme CO_2 levels on tropical climate: A CGCM study. Clim Dyn 31: 743–758

Deser C, Alexander MA, Xie SP, Phillips AS (2010) Sea Surface Temperature Variability: Patterns and Mechanisms. Ann Rev Marine Sc 2: 115–143

Grimm A (2003) The El Niño impact on the summer monsoon in Brazil: Regional processes versus remote influences. J Climate, 16, 263-280

Grimm A, Barros VR, Doyle ME (2000) Climate variability in southern South America associated with El Niño and La Niña events. J Climate, 13, 35-58

Grimm AM, Ferraz SET, Gomes J (1998) Precipitation anomalies in southern Brazil associated with El Niño and La Niña events. J Clim 11 2863–2880

Gualdi S, E Scoccimarro and A Navarra (2008) Changes in Tropical Cyclone Activity due to Global Warm-

ing: Results from a High-Resolution Coupled General Circulation Model. J Climate 21 5204-5228

Kalnay E, Kanamitsu M, Kistler R, and co-authors (1996) The NCEP/NCAR 40-Year Reanalysis Project. Bull Am Meteor Soc 77 437-471

Kidson JW (1998) Interannual variations in the southern hemisphere circulation. J Clim 1: 1177–1198

Liebmann B, and co-authors (2004) An observed trend in central South American precipitation. J Clim 17: 4357–4367

Madec, G., P. Delecluse, M. Imbard and C. Levy, 1998: OPA version 8.1 Ocean General Circulation Model reference manual. *Technical report*, LODYC/IPSL Note 11.

Mitchell TD, Jones PD (2005) An improved method of constructing a database of monthly climate observations and associated high-resolution grids. Int J Climatol 25 693–712

Navarra A, Gualdi S, Masina S, Behera S, Luo J-J, Masson S, Guilyardi E, Delecluse P, Yamagata T (2008) Atmospheric horizontal resolution affects tropical climate variability in coupled models. J Clim 21: 730–750

Mo KC, Paegle JN (2001) The Pacific-South American modes and their downstream effects. Int J Climatol 21: 1211–1229

North GR, Bell TL, Cahalan RF (1982) Sampling errors in the estimation of empirical orthogonal functions. Mon Wea Rev 110: 699–706

Paegle JN, Mo KC (2002) Linkages between summer rainfall variability over South America and sea surface temperature anomalies. J Climate, 15, 1389-1407

Pisciottano G, Diaz A, Cazes G, Mechoso CR (1994) El Niño Southern Oscillation impact on rainfall in Uruguay. J Clim 7: 1286–1302

Rayner NA, Parker DE, Horton EB, Folland CK, Alexander LV, Rowell DP, Kent EC, Kaplan A (2003) Global analysis of sea surface temperature, sea ice and night marine air temperature since the late nineteenth century. J Geophys Res 18(D14) 4407 DOI:10.1029/2002JD002670

Roeckner, E., K. Arpe, L. Bengtsson, M. Christoph, M. Claussen, L. Dümenil, M. Esch, M. Giorgetta, U. Schlese and U. Schulzweida, 1996: The Atmospheric general circulation Model ECHAM4: Model description and simulation of present-day climate: *Max-Planck Institut für Meteorologie*, Report no. 218, Hamburg, 86 pp.

Seager R, Naik N, Baethgen W, Robertson A, Kushnir Y, Nakamura J, Jurburg S (2010) Tropical oceanic causes of interannual to multidecadal precipitation variability in Southeast South America over the past century. J Climate, 23, 5517-5539

Silva GAM, Ambrizzi T, Marengo JA (2009) Observational evidences on the modulation of the South

American Low Level Jet east of the Andes according the ENSO variability. Ann Geophys 27: 645–657

Silvestri GE (2004) El Niño signal variability in the precipitation over Southeastern South America during austral summer. Geophys Res Lett 31 doi:10.1029/2004GL020590

Silvestri G, Vera C (2009) Non-stationarity impacts of the Southern Annular Mode on Southern Hemisphere climate. J Climate, 22, 6142-6148

Silvestri G, Vera C (2008) Evaluation of the WCRP-CMIP3 model simulations in the La Plata basin. Met Appl, 15, 497-502

Stuck J, A Guntner, B Merz (2006) ENSO impact on simulated South American hydro-climatology. Adv in Geosciences 6: 227–336

Solman SA, Orlanski I (2009) Subpolar high anomaly preconditioning precipitation over South America. J Atmos Sci 67: 1526–1542

Taschetto AS, Wainer I (2008) The impact of subtropical South Atlantic SST on South America precipitation. Ann Geophys 26: 3457–3476

Taschetto AS, Ambrizzi T (2012) Can Indian Ocean SST anomalies influence South American rainfall? Clim Dyn 38: 1615–1628 DOI:10.1007/s00832-0111-1165-3

Vera C, Silvestri G (2009) Precipitation interannual variability in South America from the WCRP-CMIP3 multi-model dataset. Clim Dyn, 32, 1003-1014

Vera C, Silvestri G, Liebmann B, Gonzalez P (2006) Climate change scenarios for seasonal precipitation in South America from the IPCC AR4 models. Geophys Res Lett, 33, L13707, DOI:10.1029/2006GL025759

Vera C, Silvestri G, Barros V, Carril AF (2004) Differences in El Niño response over the Southern Hemisphere. J Climate, 17, 1741–1753

Wilks DS (1995) Statistical Methods in the Atmospheric Sciences. Academic Press, 467 pp.

Wu R, Kirtman BP (2004) Impact of the Indian Ocean on the Indian summer monsoon-ENSO relationship. J Clim 17: 3037–3054

Xie P, Arkin PA (1997) Global precipitation: A 17-year monthly analysis based on gauge observations, satellite estimates, and numerical model outputs. Bull Amer Meteor Soc 78: 2539–2558

Yulaeva E, Wallace JM (1994) The signature of ENSO in global temperature and precipitation fields derived from the Microwave Sounding Unit. J Clim 7: 1719–1736

Zamboni L, Kucharski F, Mechoso CR (2012) Seasonal variations of the links between the interannual variability of South America and the South Pacific. Clim Dyn 38(9): 2115–2129 DOI 10.1007/s00382-011-1116-zn

599 Zamboni L, Mechoso CR, Kucharski F (2010) Relationships between upper-level circulation over South
600 America and rainfall over Southeastern South America: A physical base for seasonal predictions. J Clim
601 23: 3300–3315
602 Zhou J, Lau KM (2001) Principal modes of interannual and decadal variability of summer rainfall over
603 South America. Int J Climatol 21: 1623–1644
604 Zhou J, Lau KM (2002) Intercomparison of model simulations of the impact of 1997/98 El Niño on South
605 American summer monsoon. Meteorologica 27: 99–116

606 ## Tables

Table 1. OND mean precipitation and its standard deviation (mm/d) averaged over the South American continent (SA) between 45°S and the Equator, and over the La Plata Basin (LPB) region (65°-47°W, 37°-19°S) for CRU dataset (first row), AMIP-type ensemble (second row) and coupled model experiment (SSXX, third row).

Precip (mm/d)	SA OND mean	SA OND std	LPB OND mean	LPB OND std
CRU	4.52	0.44	4.12	1.02
AMIP-type	4.35	0.31	4.68	0.80
SSXX	4.26	0.77	4.44	0.88

Table 2. Correlation coefficients between rotated principal components (RPC1, RPC2 and RPC3) of South America OND precipitation anomalies in CRU and CMAP datasets for the period 1979-2005. An asterisk marks the values that are statistically significant at 95%.

	RPC1(CRU)	RPC2(CRU)	RPC3(CRU)
RPC1(CMAP)	0.95*	-0.07	-0.19
RPC2(CMAP)	-0.10	0.63*	+0.20
RPC3(CMAP)	+0.32	-0.10	0.79*

Table 3. Correlation coefficients between NINO3.4 index and OND SA precipitation rotated principal component (RPC1) for the AMIP-type ensemble. Values are reported for each member (from #1 to #9) of the ensemble.

	#1	#2	#3	#4	#5	#6	#7	#8	#9
RPC1	0.44	0.13	0.15	0.47	0.20	0.27	0.28	0.36	0.53

Table 4. Anomalies of vertical velocity (ω, mb/s) at 500 mb in the region Eq-20°S, 75°W-55°W (2nd column) and of zonal velocity (m/s) at 200 mb in the region 20°S-40°S, 90°W-60°W (3rd column) for the "In Phase", "Out of Phase" and "Partial in Phase" composites in positive and negative cases (from top to bottom).

	ω 500 (mb/s)	u200 (m/s)
In Phase Pos	0.65	2.82
Out Phase Pos	0.09	1.35
Partial Phase Pos	0.19	2.27
In Phase Neg	-0.26	-0.84
Out Phase Neg	-0.08	-0.17
Partial Phase Neg	-0.21	-0.75

Table 5. List of years where the model RPC1 is "In Phase" (exceeding 1 standard deviation in the same direction) or "Out of Phase" (exceeding 1 standard deviation in the opposite direction) with the CRU RPC1. Years are separated for wet LPB years (i.e. positive RPC1 values) and for dry LPB years (i.e. negative RPC1 values). Within each year the number of members having the same behavior is indicated in parentheses. The years in **bold** are discussed with more details in section 5.

	Wet LPB Years	Dry LPB Years
In Phase	1951(4) 1963(1) **1982(9)** 1997(4) 2002(5)	1971(1) 1985(2) 1989(2) **1999(4)**
Out of Phase	1961(3) 1963(2) 1997(1) 2002(2) **2003(8)**	1948(6) 1955(3) 1956(4) 1962(4) 1971(3) 1985(2)

Figure Captions

Fig. 1. First three rotated EOFs of OND mean South American precipitation (in the box shown considering land-points only) for (a,b,c) CRU and (d,e,f) CMAP datasets in the period 1979-2005. The percentage of variance explained by each mode is shown in parentheses (top of each panel).

Fig. 2. First rotated EOF modes of OND South American precipitation (as in fig. 1) for (a) CRU dataset from 1948 to 2003 and (b) AMIP-type ensemble. The percentage of explained variance is in parentheses at the top of each panel. (c) RPC1 for the CRU dataset.

Fig. 3. Time-correlation coefficients of OND South America precipitation RPC1 and OND SST for (a) HadISST/CRU datasets, (b) AMIP-type ensemble, and (c) coupled model experiment (SSXX).

Fig. 4. Composite anomalies of SST (°C, shaded) and 200 mb eddy streamfunction (10^6 m^2/s, contours) for wet (left panels) and dry (right panels) LPB years in (a,b) HadISST/CRU datasets and (c,d) AMIP-type ensemble. Shaded and thicker contours are statistically significant at 95%.

Fig. 5. Composite anomalies of precipitation (mm/d) for wet (positive cases, upper panels) and dry (negative cases, lower panels) LPB years in the AMIP-type ensemble grouped as (a,b) "In Phase", (c,d) "Out of Phase" and (e,f) "Partial in Phase" RPC1 values (the classification is described in the text). The values shown are statistically significant at 95%.

Fig. 6. Composite anomalies of SST (°C, shaded) and 200 mb eddy streamfunction (10^6 m^2/s, contours) for wet (positive cases, left panels) and dry (negative cases, right panels) LPB years in the AMIP-type ensemble grouped as (a,b) "In Phase", (c,d) "Out of Phase" and (e,f) "Partial in Phase" RPC1 values (the classification is described in the text). Shaded and thicker contours are statistically significant at 95%.

Fig. 7. Same as fig. 5 but for vertically integrated moisture (kg/m^2, shaded) and vertically integrated moisture flux (kg/m s, vectors). The values shown are statistically significant at 95%.

Fig. 8. OND 1982 anomalies of (a) SST (°C, shaded) and 200 mb eddy streamfunction (10^6 m^2/s, contours), (b) precipitation (mm/d, shaded) for the AMIP-type ensemble.

Fig. 9. OND 2003 anomalies of (a,c) SST (°C, shaded) and 200 mb eddy streamfunction (10^6 m^2/s, contours), (b,d) precipitation (mm/d) for HadISST/CRU/NCEP datasets and AMIP-type ensemble, respectively.

Fig. 10. OND 2003 200 mb eddy streamfunction (10^6 m^2/s) anomalies for (a-i) each member of the AMIP-type ensemble (from #1 to #9). (l) OND inter-members standard deviation of 200 mb streamfunction (10^6 m^2/s).

Fig. 11. OND 1999 anomalies of (a,c) SST (°C, shaded) and 200 mb eddy streamfunction (10^6 m^2/s, contours), (b,d) precipitation (mm/d) for HadISST/CRU/NCEP datasets and AMIP-type ensemble, respectively.

Fig. 12. OND 1999 precipitation (mm/d, shaded) and 200 mb eddy streamfunction (10^6 m^2/s, contours) anomalies for (a-i) each member of the AMIP-type ensemble (from #1 to #9). (l) OND inter-members standard deviation of 200 mb streamfunction (10^6 m^2/s).

608 **Figures**

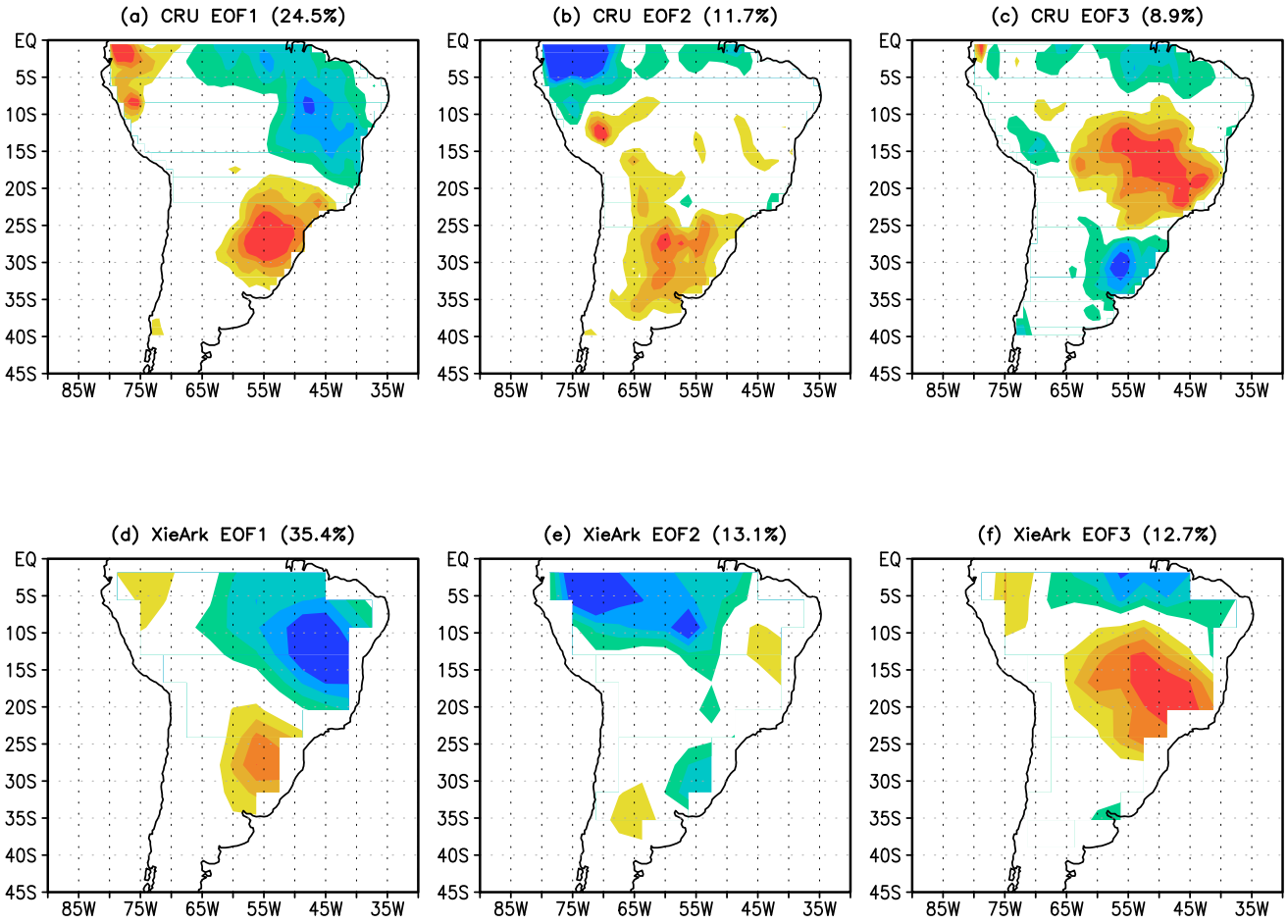

Fig. 1. First three rotated EOFs of OND mean South American precipitation (in the box shown considering land-points only) for (a,b,c) CRU and (d,e,f) CMAP datasets in the period 1979-2005. The percentage of variance explained by each mode is shown in parentheses (top of each panel).

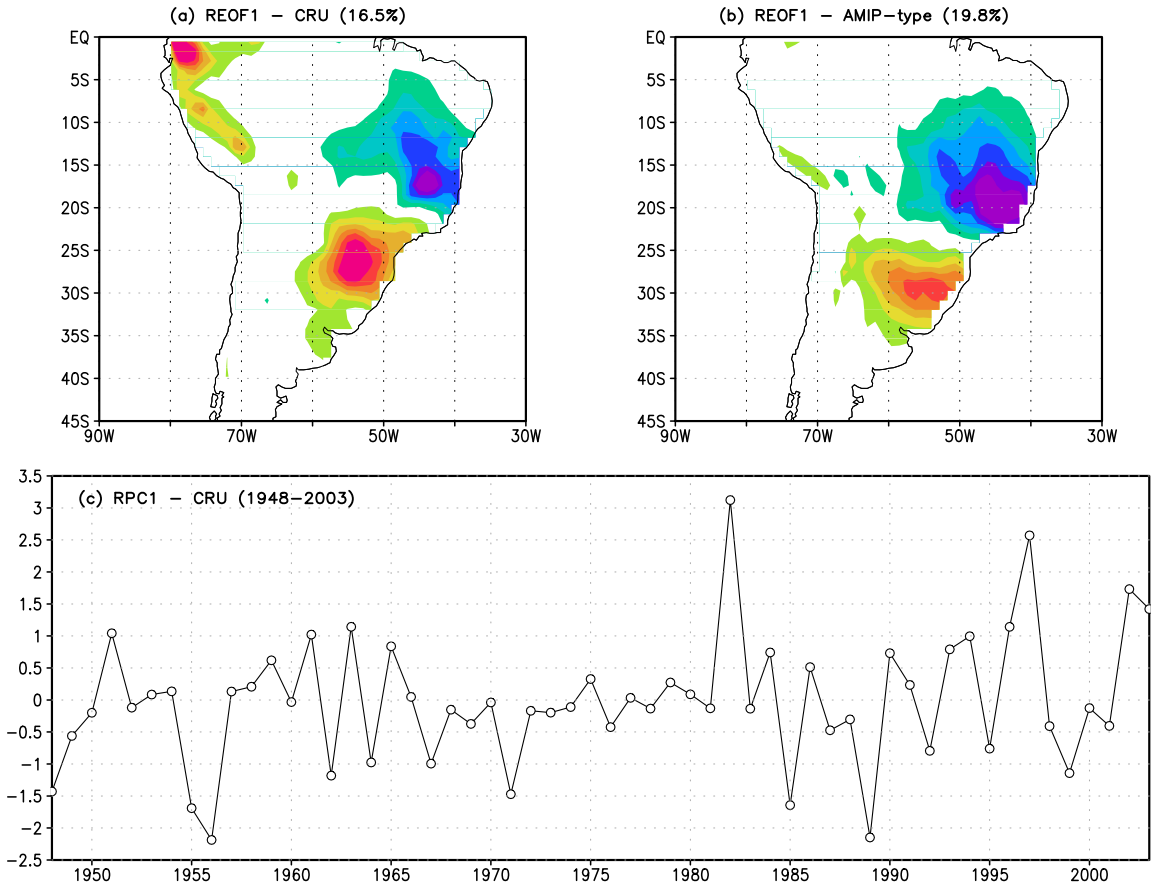

Fig. 2. First rotated EOF modes of OND South American precipitation (as in fig. 1) for (a) CRU dataset from 1948 to 2003 and (b) AMIP-type ensemble. The percentage of explained variance is in parentheses at the top of each panel. (c) RPC1 for the CRU dataset.

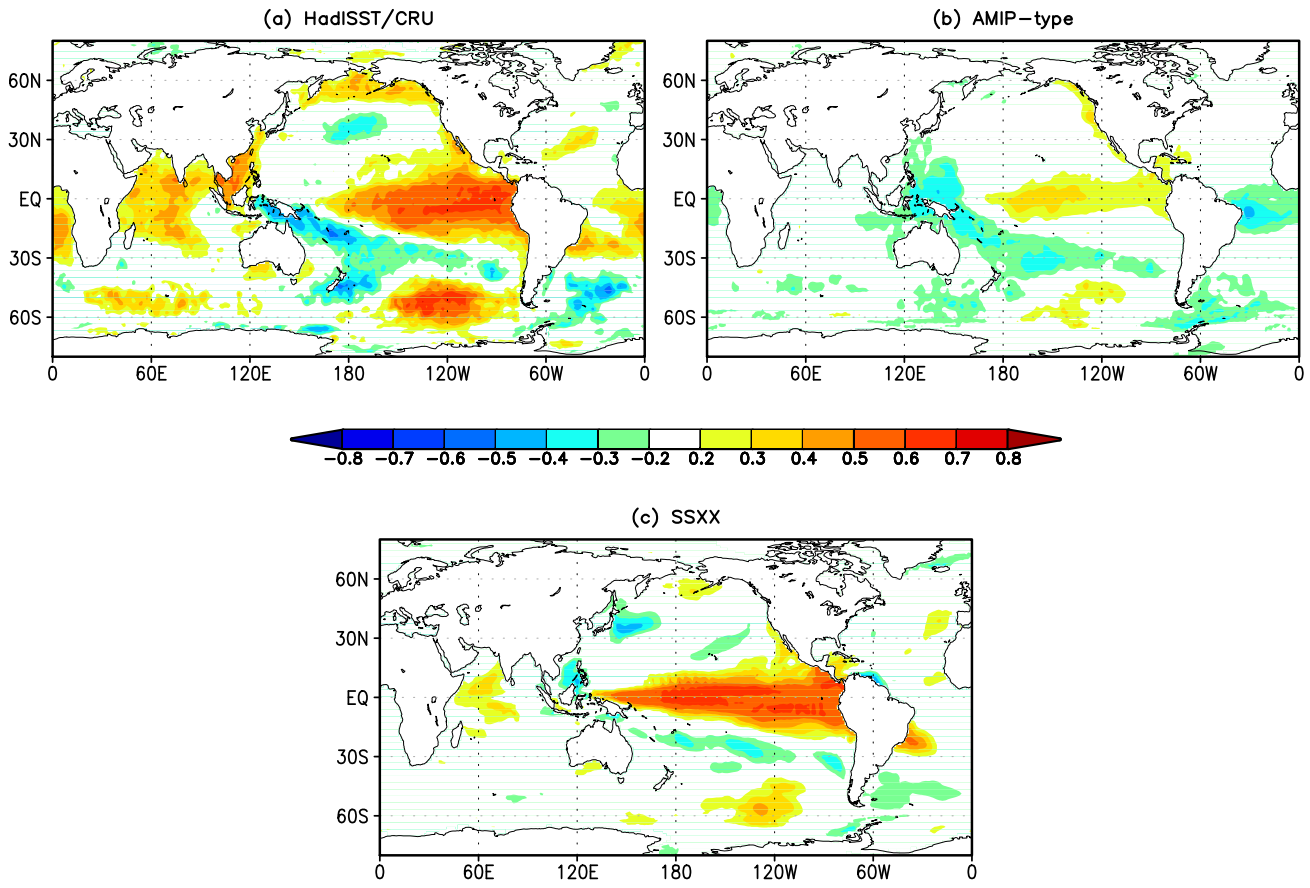

Fig. 3. Time-correlation coefficients of OND South America precipitation RPC1 and OND SST for (a) HadISST/CRU datasets, (b) AMIP-type ensemble, and (c) coupled model experiment (SSXX).

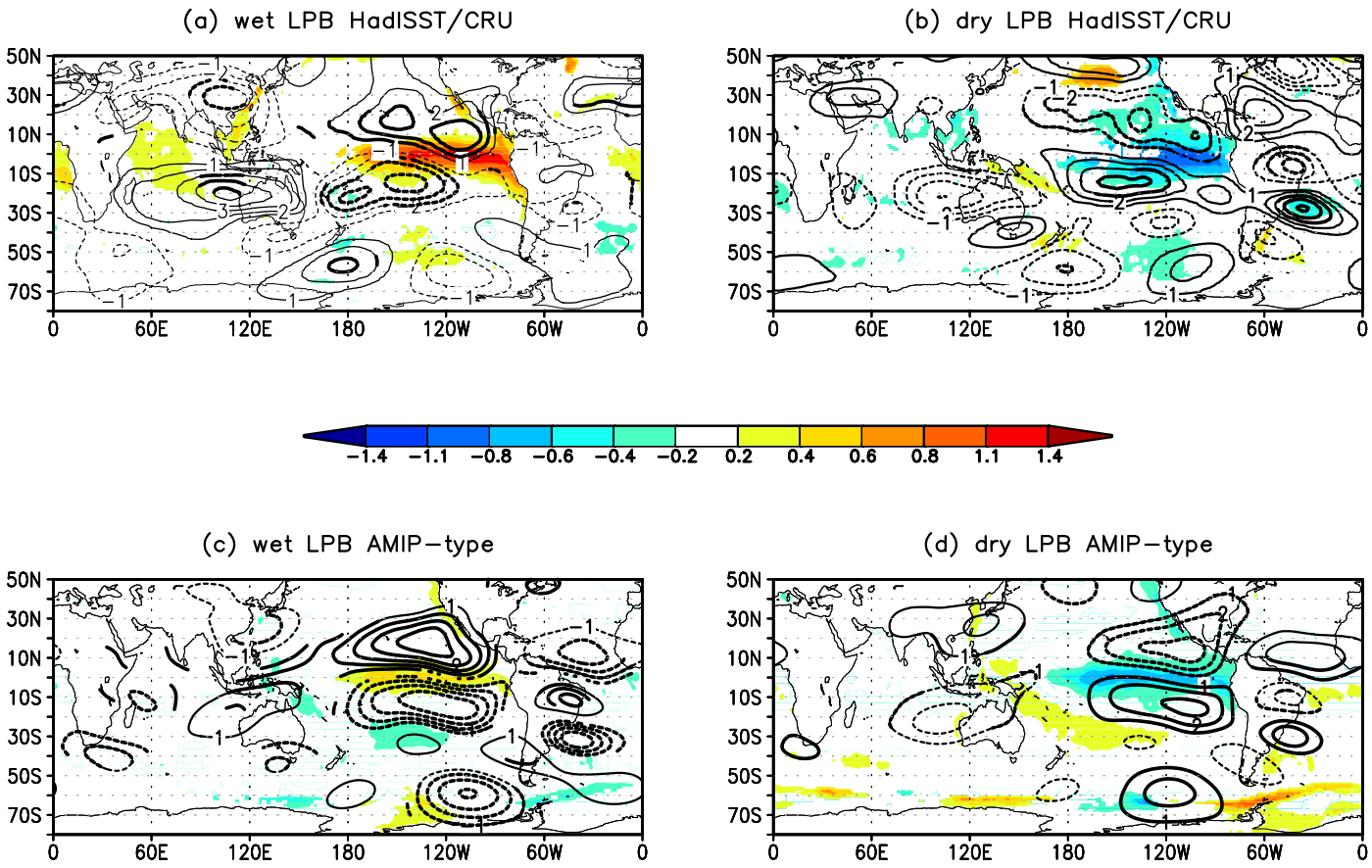

Fig. 4. Composite anomalies of SST (°C, shaded) and 200 mb eddy streamfunction (10^6 m^2/s, contours) for wet (left panels) and dry (right panels) LPB years in (a,b) HadISST/CRU datasets and (c,d) AMIP-type ensemble. Shaded and thicker contours are statistically significant at 95%.

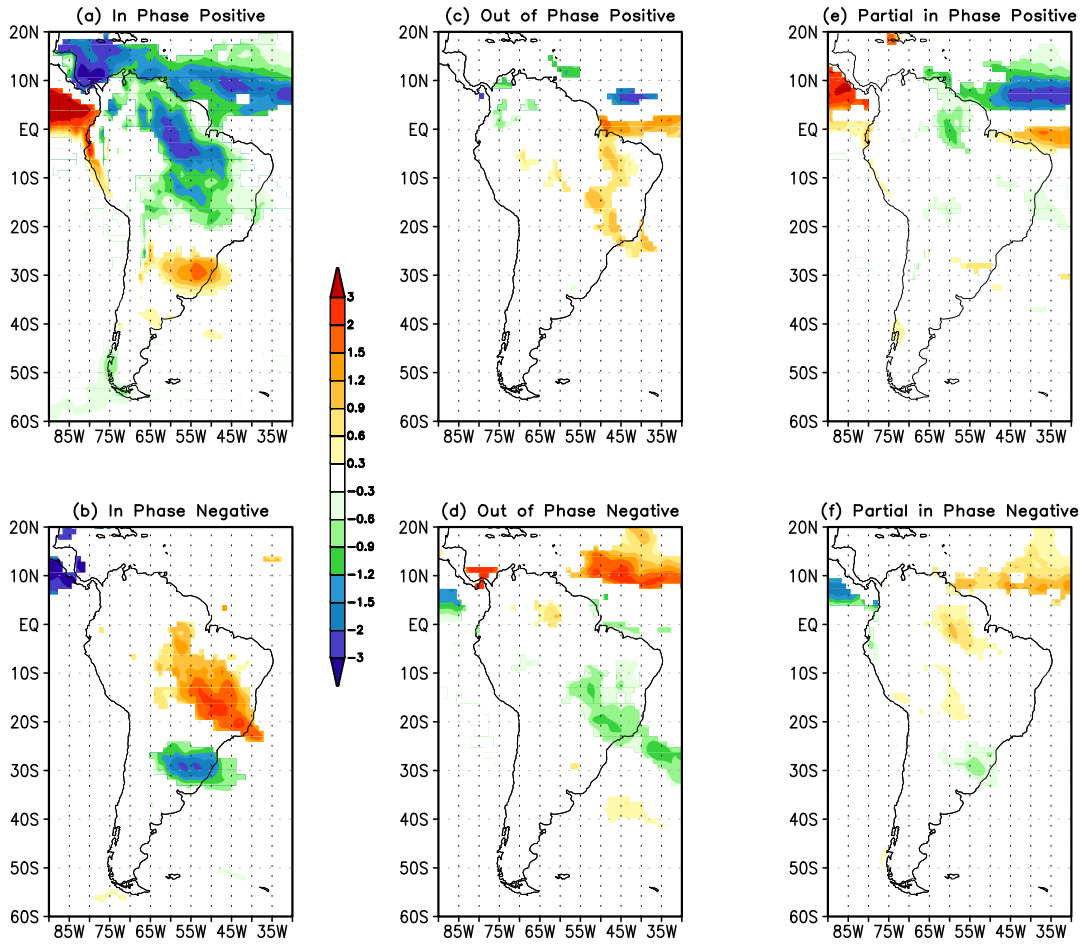

Fig. 5. Composite anomalies of precipitation (mm/d) for wet (positive cases, upper panels) and dry (negative cases, lower panels) LPB years in the AMIP-type ensemble grouped as (a,b) "In Phase", (c,d) "Out of Phase" and (e,f) "Partial in Phase" RPC1 values (the classification is described in the text). The values shown are statistically significant at 95%.

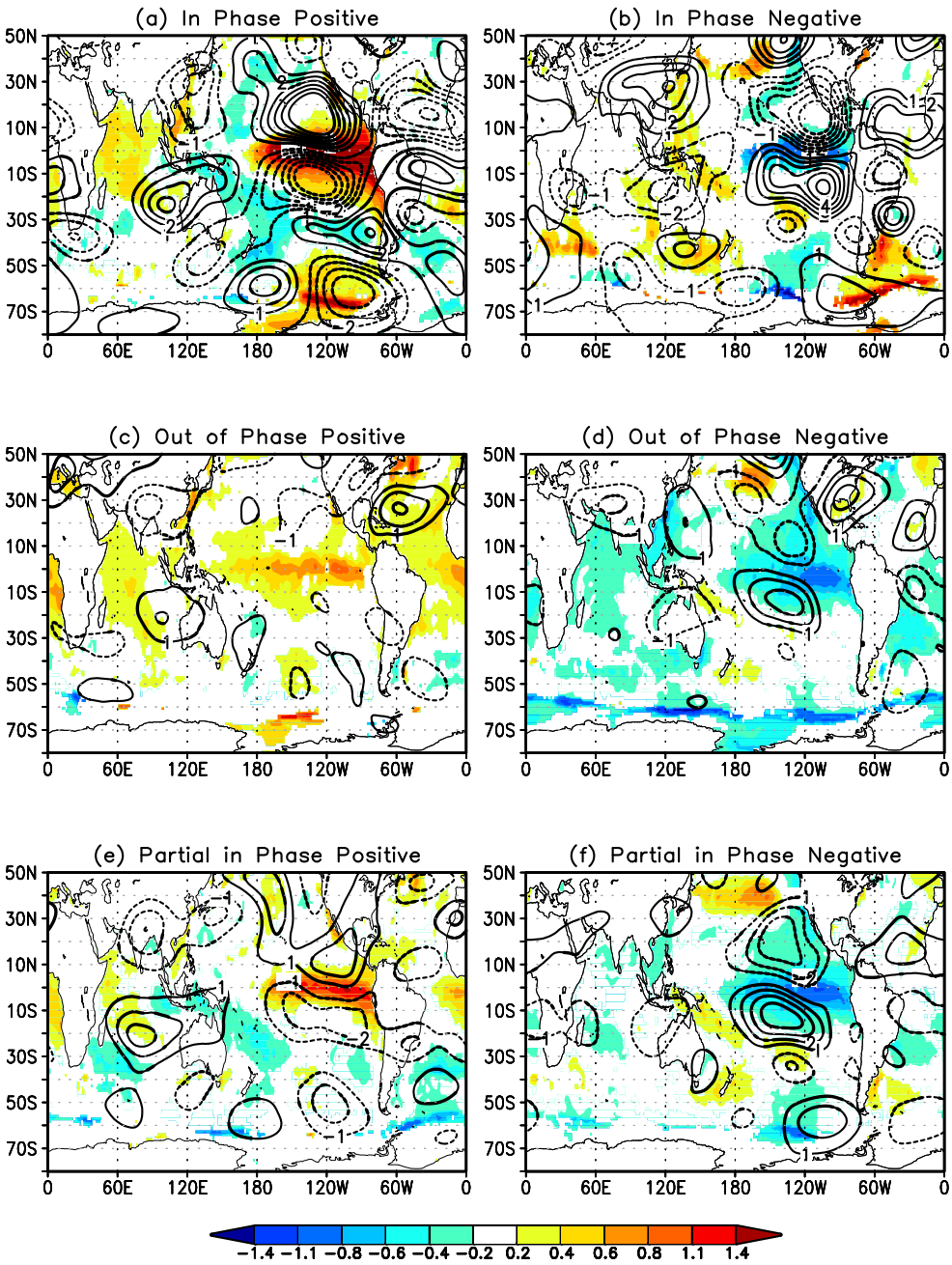

Fig. 6. Composite anomalies of SST (°C, shaded) and 200 mb eddy streamfunction (10^6 m^2/s, contours) for wet (positive cases, left panels) and dry (negative cases, right panels) LPB years in the AMIP-type ensemble grouped as (a,b) "In Phase", (c,d) "Out of Phase" and (e,f) "Partial in Phase" RPC1 values (the classification is described in the text). Shaded and thicker contours are statistically significant at 95%.

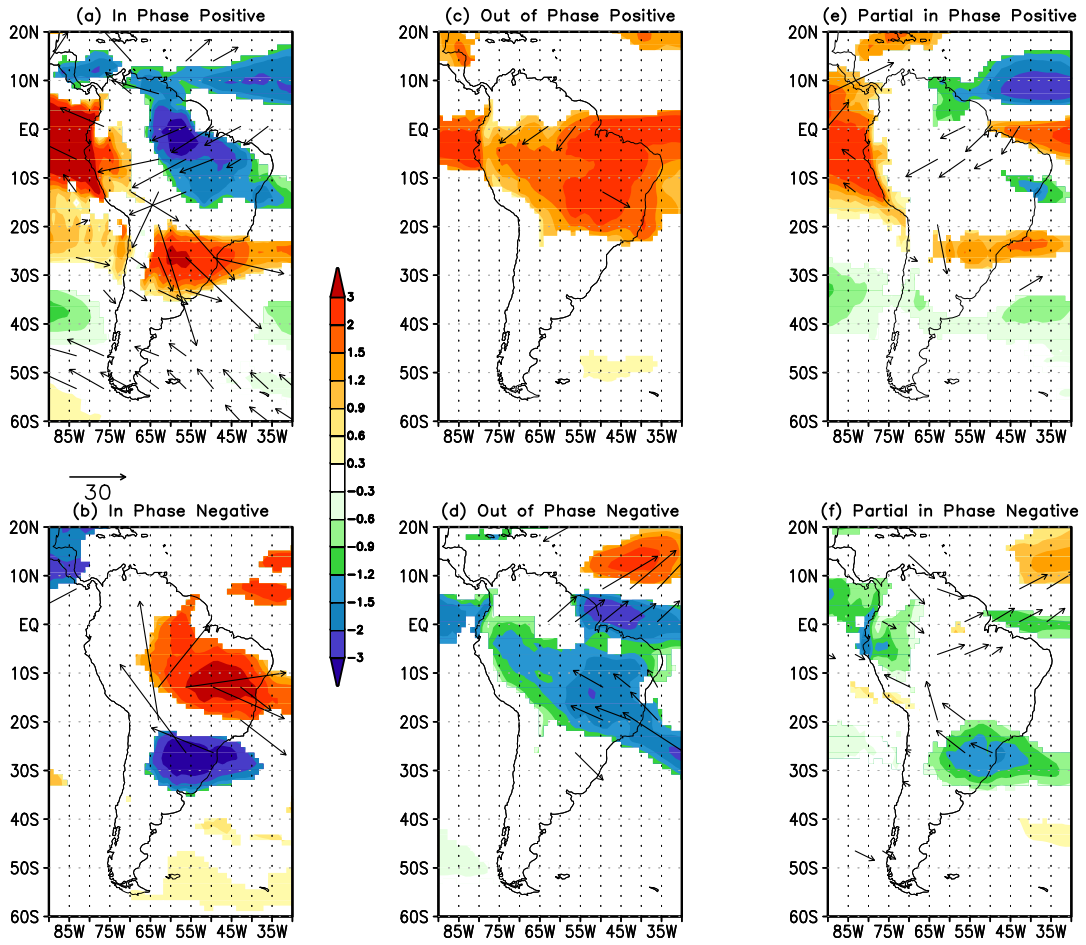

Fig. 7. Same as fig. 5 but for vertically integrated moisture (kg/m^2, shaded) and vertically integrated moisture flux (kg/m s, vectors). The values shown are statistically significant at 95%.

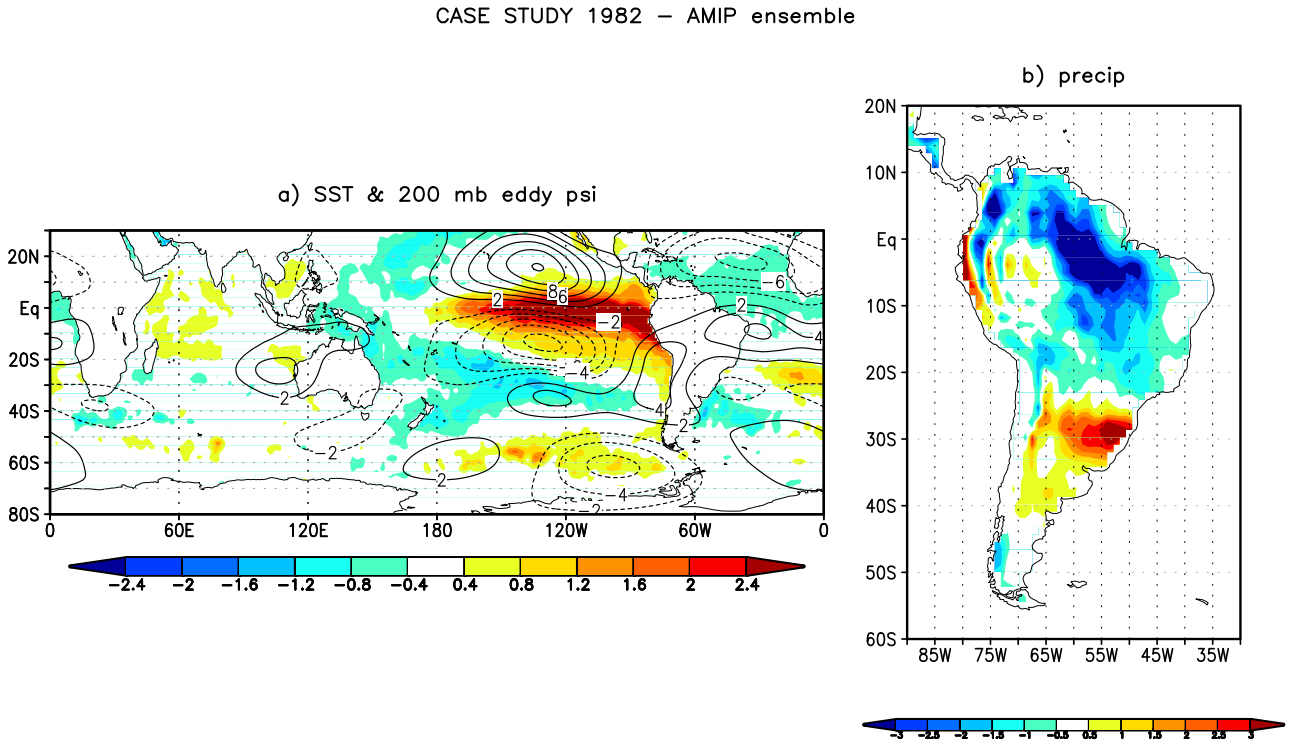

Fig. 8. OND 1982 anomalies of (a) SST (°C, shaded) and 200 mb eddy streamfunction (10^6 m^2/s, contours), (b) precipitation (mm/d, shaded) for the AMIP-type ensemble.

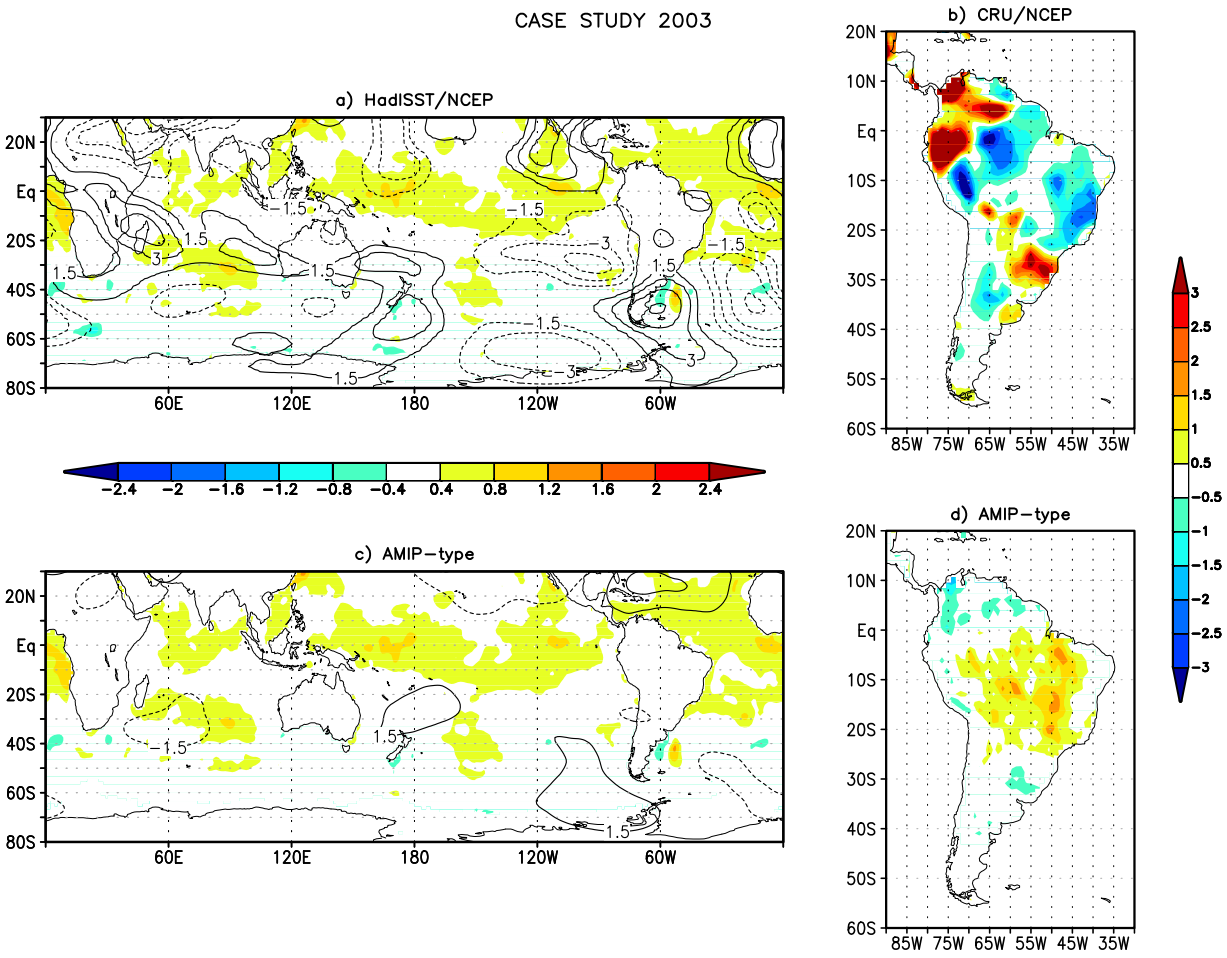

Fig. 9. OND 2003 anomalies of (a,c) SST (°C, shaded) and 200 mb eddy streamfunction (10^6 m^2/s, contours), (b,d) precipitation (mm/d) for HadISST/CRU/NCEP datasets and AMIP-type ensemble, respectively.

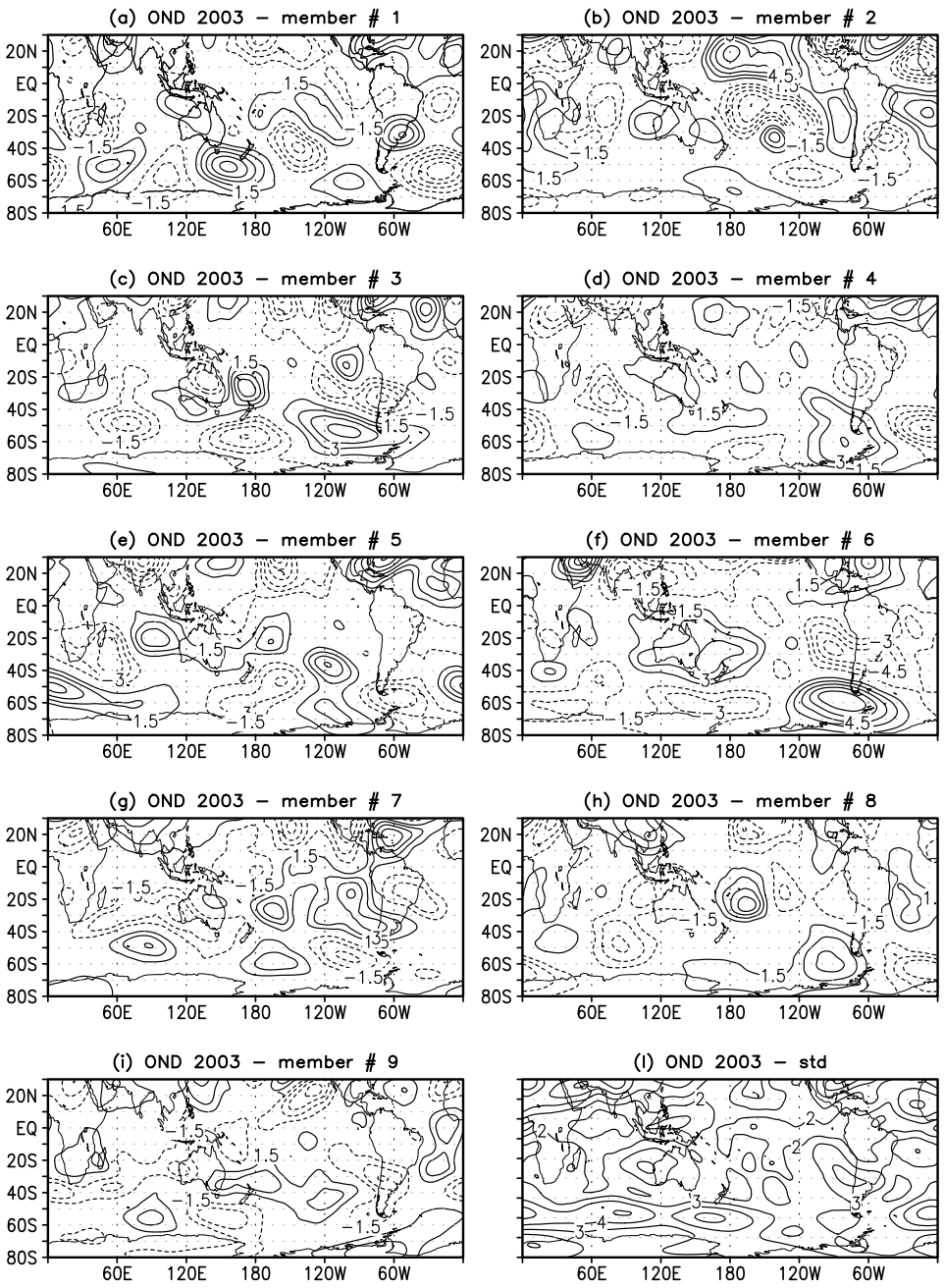

Fig. 10. OND 2003 200 mb eddy streamfunction (10^6 m^2/s) anomalies for (a-i) each member of the AMIP-type ensemble (from #1 to #9). (l) OND inter-members standard deviation of 200 mb streamfunction (10^6 m^2/s).

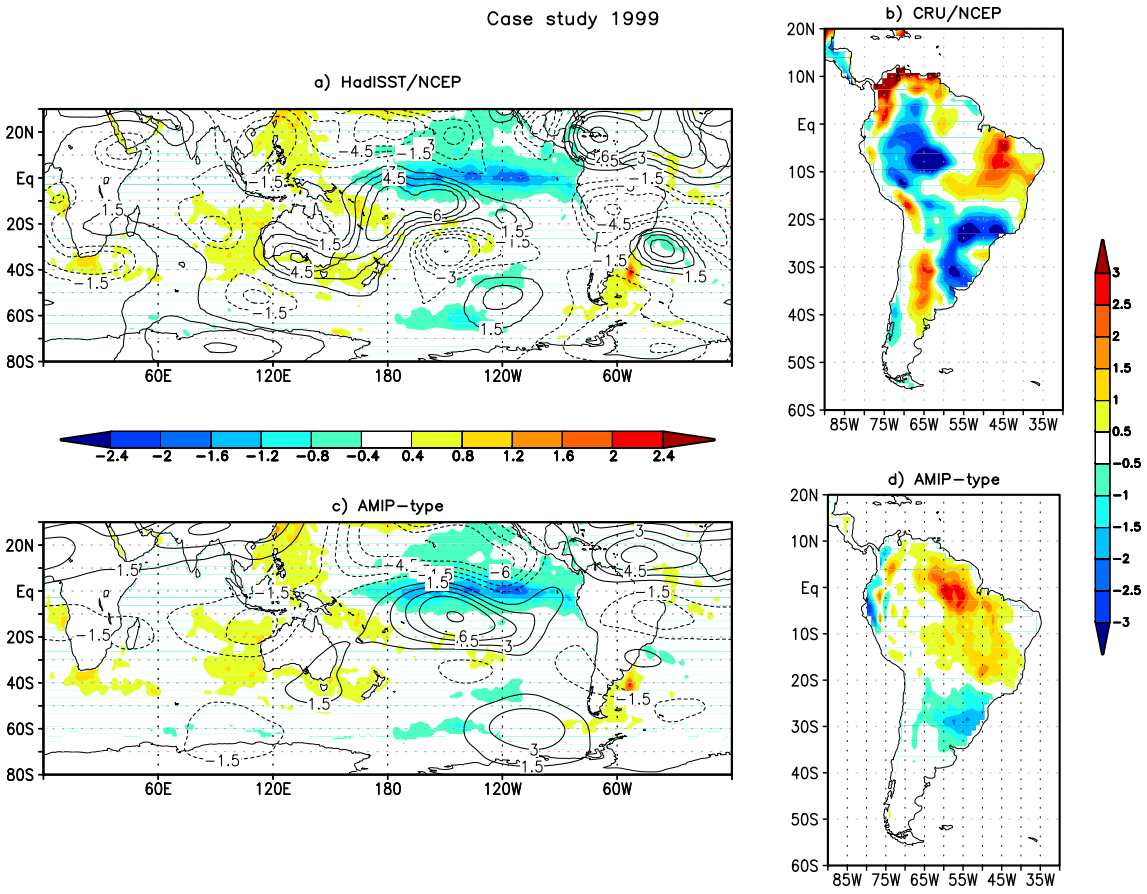

Fig. 11. OND 1999 anomalies of (a,c) SST (°C, shaded) and 200 mb eddy streamfunction (10^6 m^2/s, contours), (b,d) precipitation (mm/d) for HadISST/CRU/NCEP datasets and AMIP-type ensemble, respectively.

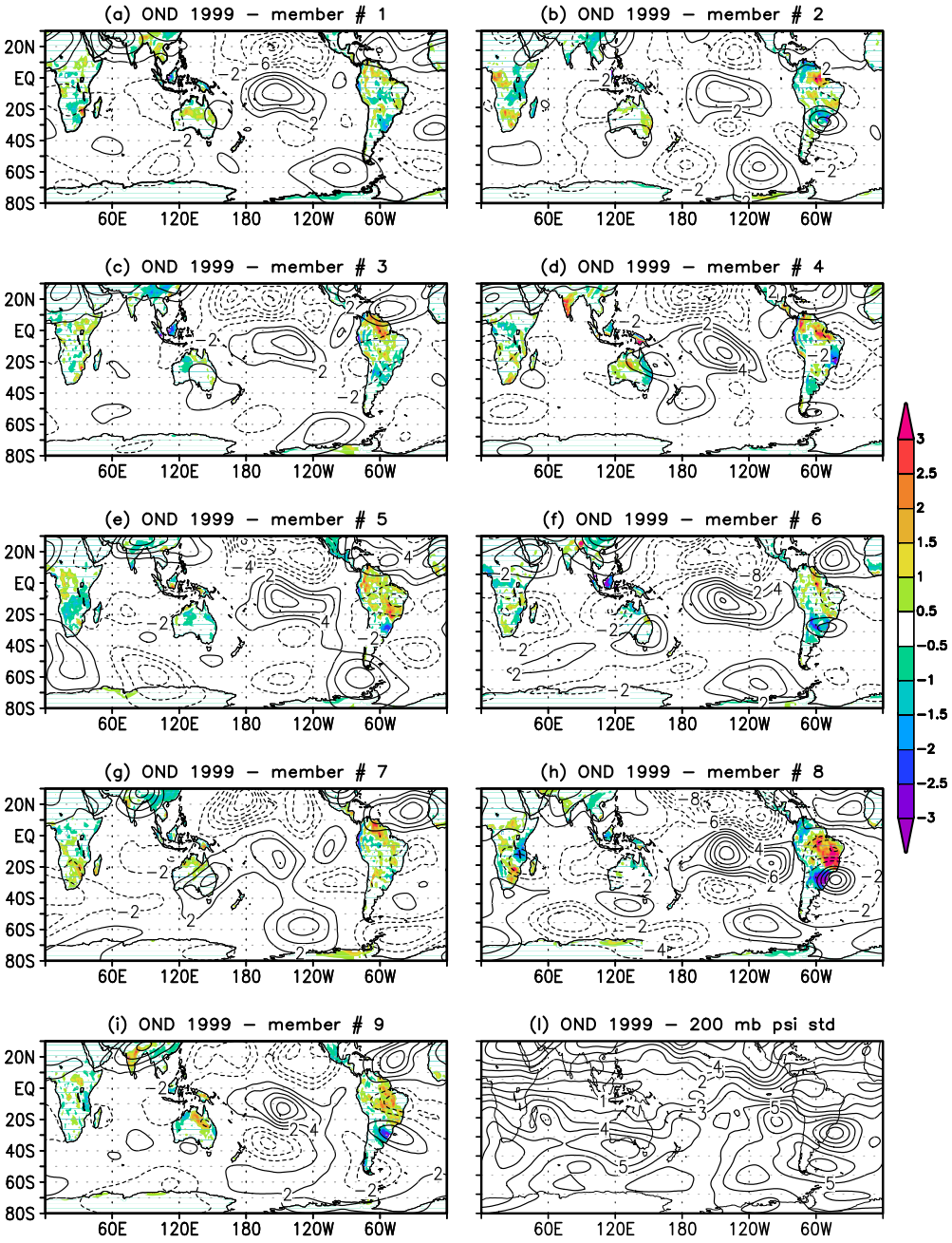

Fig. 12. OND 1999 precipitation (mm/d, shaded) and 200 mb eddy streamfunction (10^6 m^2/s, contours) anomalies for (a-i) each member of the AMIP-type ensemble (from #1 to #9). (l) OND inter-members standard deviation of 200 mb streamfunction (10^6 m^2/s).